An engineered muscle flap for reconstruction of large soft tissue defects

Yulia Shandalov[a,1], Dana Egozi[b,c,1], Jacob Koffler[a,d], Dekel Dado-Rosenfeld[a], David Ben-Shimol[b], Alina Freiman[a,d], Erez Shor[a], Aviva Kabala[a], and Shulamit Levenberg[a,2]

[a]Biomedical Engineering and [b]Medicine Departments and [d]Interdepartmental Program in Biotechnology, Technion—Israel Institute of Technology, Haifa 32000, Israel; and [c]Department of Plastic and Reconstructive Surgery, Rambam Health Care Campus, Haifa 31096, Israel

Edited by Robert Langer, Massachusetts Institute of Technology, Cambridge, MA, and approved March 7, 2014 (received for review February 13, 2014)

Large soft tissue defects involve significant tissue loss, requiring surgical reconstruction. Autologous flaps are occasionally scant, demand prolonged transfer surgery, and induce donor site morbidity. The present work set out to fabricate an engineered muscle flap bearing its own functional vascular pedicle for repair of a large soft tissue defect in mice. Full-thickness abdominal wall defect was reconstructed using this engineered vascular muscle flap. A 3D engineered tissue constructed of a porous, biodegradable polymer scaffold embedded with endothelial cells, fibroblasts, and/or myoblasts was cultured in vitro and then implanted around the femoral artery and veins before being transferred, as an axial flap, with its vascular pedicle to reconstruct a full-thickness abdominal wall defect in the same mouse. Within 1 wk of implantation, scaffolds showed extensive functional vascular density and perfusion and anastomosis with host vessels. At 1 wk posttransfer, the engineered muscle flaps were highly vascularized, were well-integrated within the surrounding tissue, and featured sufficient mechanical strength to support the abdominal viscera. Thus, the described engineered muscle flap, equipped with an autologous vascular pedicle, constitutes an effective tool for reconstruction of large defects, thereby circumventing the need for both harvesting autologous flaps and postoperative scarification.

tissue engineering | vascularization | reconstructive surgery | tissue regeneration

Successful restoration of substantial large soft tissue defects, caused by severe trauma or cancer ablation, poses a significant clinical challenge (1). The current therapeutic approach involves grafts, synthetic material replacement, and autologous tissue transfer by means of tissue flaps. Tissue grafts are ineffective in repairing large defects (2) because of the absence of blood supply, and they resorb or necrose when postimplantational vascularization is not established (3–5). In contrast, flaps are autologous tissues that can be transferred with their own blood supply and therefore, preferred for repair of large defects. However, the duration of the surgical operation, the scant availability of quality vascularized flaps, and donor site morbidity often limit their use (6).

In recent years, the tissue engineering discipline has presented a promising approach to address these challenges by providing new sources of tissues and enabling angiogenesis into the tissue after implantation (3). Numerous works report successful generation of tissue for repair of a variety of tissue defects, such as breast reconstruction with adipose tissue (7, 8), and various aesthetic restorations in the face and the body (9–12). Successful transplantation of tissue-engineered trachea (13, 14) and bladder (15) was reported in human patients, and encouraging results were observed on transplantation of a variety of tissues, such as cornea (16), bone (17), and skin (18). However, although this approach provides a successful platform for mass generation and transplantation of thin tissues, fabrication of a thick vascularized engineered tissue bearing its own pedicle still remains an unmet challenge of tissue engineering.

The purpose of this study was to fabricate an engineered muscle flap for repair of large soft tissue defects in mice, whereas large abdominal wall defects were chosen as a proof-of-concept model. A muscle tissue was constructed in vitro by seeding myoblasts, fibroblasts, and endothelial cells onto a 3D biodegradable poly-L-lactic acid (PLLA)/poly(lactic-coglycolic acid) (PLGA) scaffold. The graft was cultured in vitro until a small capillary net was formed, which was then anastamosed in vivo with the capillaries sprouted from the recipient's femoral artery and vein. The graft was then transferred with the femoral vessels, as a flap, to cover a full-thickness abdominal wall defect. The transferred flap proved viable and well-vascularized, provided mechanical support to the abdominal wall, and became well-integrated in the surrounding tissue. Thus, the engineered tissue flap, bearing both host and human-derived blood vessels, presents a novel tool for repairing a full-thickness defect of the abdominal wall without requiring autologous muscle flap.

Results

Postimplantational viability of a large and thick engineered tissue requires nutritional support that can only be provided by a large blood vessel. For this purpose, grafts constructed of a porous, biodegradable PLLA/PLGA scaffold embedded with endothelial cells (ECs), fibroblasts, and/or myoblasts (Fig. 1*A*) were cultured for 10 d and then folded around the host's artery and vein (AV) while being separated from the surrounding tissue by a piece of sterile latex (Fig. 1 *B* and *E–I*). One and two weeks postimplantation, the graft with the AV was transferred to the abdominal full-thickness wall defect as an axial flap (Fig. 1 *C*, *D*, and *J–N*).

Significance

Effective restoration of large soft tissue defects requires the use of tissue flaps, with viability that is largely determined by degree of vascularization. In view of the tedious transfer procedures and donor site morbidity associated with autologous flaps, this work set out to design and evaluate an engineered muscle flap featuring a robust vascular port formed from preseeded endothelial cells and host vasculature. The implanted flap was highly vascularized, well-perfused, and anastomosed with host vessels. Engineered flaps of this nature promise to circumvent the need to harvest and transfer massive tissue volumes, while avoiding the consequential complications.

Author contributions: Y.S., D.E., J.K., D.D.-R., and S.L. designed research; Y.S., D.E., J.K., D.D.-R., A.F., and A.K. performed research; E.S. contributed new reagents/analytic tools; Y.S., D.E., J.K., D.D.-R., D.B.-S., E.S., and S.L. analyzed data; and Y.S., D.E., and S.L. wrote the paper.

The authors declare no conflict of interest.

This article is a PNAS Direct Submission.

[1]Y.S. and D.E. contribute equally to this work.

[2]To whom correspondence should be addressed. E-mail: shulamit@bm.technion.ac.il.

This article contains supporting information online at www.pnas.org/lookup/suppl/doi:10.1073/pnas.1402679111/-/DCSupplemental.

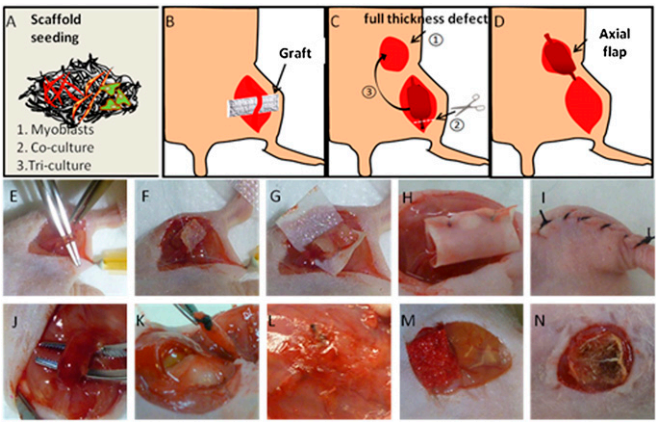

Fig. 1. Surgical implantation of fabricated tissue grafts followed by flap transfer. (*A–D*) Schematic presentation of flap fabrication. (*A*) Cells were seeded within biodegradable PLLA/PLGA scaffolds. (*B*) The fabricated tissue graft was folded around the blood vessels and sutured. (*C* and *D*) Transfer of the vascularized graft into the abdominal wall defect. (*E*) Isolation of the femoral artery and vein from the surrounding tissue. (*F*) The fabricated tissue graft was folded around the blood vessels and sutured. (*G* and *H*) The fabricated tissue graft was then separated from the skin and the surrounding tissue using a piece of sterile latex, which was then sutured. (*I*) Suturing of the overlying skin. (*J*) Representative image of a fabricated tissue graft 1 wk after its implantation. (*K*) Transfer of the vascularized graft into the abdominal wall defect. (*L*) Appearance of the flap derived from cell-embedded scaffolds at 1 wk after transfer; the flap is vascularized and viable. (*M*) Image of a piece of a cell-free scaffold applied to close the abdominal wall defect. (*N*) Appearance of a graft derived from a cell-free scaffold 1 wk after the transfer; the graft had become necrotic.

Analysis of Graft Integration and Vascularization. Three types of fabricated grafts were prepared consisting of (*i*) myoblasts (Myo graft), (*ii*) ECs and fibroblasts (EC/Fib graft), or (*iii*) ECs, fibroblasts, and myoblasts (EC/Fib/Myo graft), and they were designed to most closely mimic the composition of a muscle tissue. An empty scaffold was used as a control. The viability and vascularization of the grafts were assessed 1 and 2 wk after implantation.

Macroscopically, within 1 wk of implantation, all grafts appeared viable and had already become vascularized (Fig. 1*J*), and new functional blood vessels had sprouted from the AV to the engineered tissue graft (Fig. 2 *A–D*). Many capillaries were observed in the tissue surrounding the AV, suggesting that the scaffolds had integrated with the host tissue. EC/Fib/Myo grafts were most highly vascularized, which was indicated by the mean vasculature density of CD31-positive vessels per millimeters^2 (Fig. 2*E* and Fig. S1) and significantly higher than that observed in the Myo, EC/Fib, and empty grafts (Fig. 2 *G–I*). At 2 wk postimplantation, both the EC/Fib/Myo and Myo grafts were highly vascularized, with similar densities of CD31-positive vessels (Fig. *2F*) and no significant differences seen when using either C2C12 myoblasts or primary myoblasts (Fig. S2*A*). In contrast, vascularization of the EC/Fib and empty grafts remained low (Fig. 2*F*).

An i.v. injection of a mixture of *Ulex europaeus* agglutinin I and *Griffonia simplifolia* isolectin B4 was administered to determine whether the vascular network of the engineered tissue graft had anastomosed with host vessels and identify perfused and functional blood vessels (19, 20). Two patterns of double staining confirmed perfusion within the vessels and included either human umbilical vein endothelial cells (HUVECs) wrapped around host blood vessels or long human-derived vessels that had anastomosed with host blood vessels (Fig. 2 *J* and *K*). Most of the blood vessels found in the graft area were mouse-derived vessels.

Analysis of Graft Perfusion and Vascularization. Vessel patency and the extent of vascularization and neovasculature within the grafts were assessed by injection of FITC-Dextran into the tail vein and analysis of the functional vessel density (FVD) from confocal images of the graft areas (Fig. 3 *A–C* and Movie S1, Doppler). One week after implantation, the FVD of the EC/Fib/Myo grafts was markedly higher than that of both the Myo and EC/Fib grafts (Fig. 3 *A*, *a–c*; *B*, *a–c*; *C*, *a–c*; and *D* and Fig. S2*B*). However, 2 wk after implantation, the FVD of Myo and EC/Fib/Myo grafts was similar, whereas the FVD of the EC/Fib grafts remained stable (Fig. 3 *A*, *d–f*; *B*, *d–f*; *C*, *d–f*; and *E*).

Ultrasonigraphic evaluation of graft perfusion rate and the perfused vascular volume showed perfusion within the EC/Fib/Myo grafts at 1 and 2 wk postimplantation, which was expressed by the low number of orange pixels within the graft immediately after the disruption pulse of the microbubbles (outlined in Fig. 4*A*) and a signal increase 25 s later (Fig. 4 *B* and *C*, EC/Fib/Myo

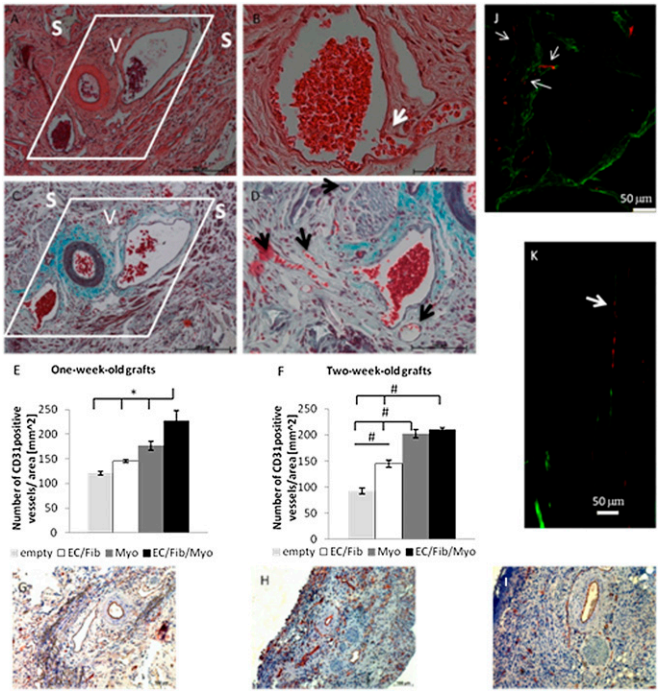

Fig. 2. Sprouting of new functional vessels with red blood cells from the host's femoral artery and vein to the engineered tissue graft. (*A* and *B*) H&E staining. (*C* and *D*) MT representative staining 1 wk postimplantation of the sprouting from the femoral vein to the engineered tissue. S depicts the scaffold, and V depicts the mouse artery and vein. (Scale bar: 200 μm.) (*B*) The white arrow points to a host vessel sprouting to the scaffold. (Scale bar: 50 μm.) (*D*) The black arrows point to new capillaries. (Scale bar: 100 μm.) (*E* and *F*) Vascularization quantification of EC/Fib/Myo graft vs. EC/Fib, Myo, or empty scaffolds. The density of CD31-positive vessels measured at (*E*) 1 and (*F*) 2 wk postimplantation. All values are normalized to the graft's area (millimeters^2). $^*P < 0.05$ according to the results of the posthoc Student Newman–Keuls multiple comparisons test. In *F*, all groups are significantly different from each other. $^{\#}P < 0.001$ according to the results of the posthoc Student Newman–Keuls multiple comparisons test except for the Myo vs. EC/Fib/Myo grafts. For all determinations, the sample size was $n > 3$, and all values are represented as mean ± SEM. (*G–I*) Representative images of CD31-stained blood vessels in grafts at 1 wk postimplantation (brown). (*G*) EC/Fib grafts, (*H*) Myo grafts, and (*I*) EC/Fib/Myo grafts. The nuclei are stained blue. (*J* and *K*) Anastomosis between functional human-derived vessels and host (mouse) vessels identified after a tail vein injection of a mixture of rhodamine-conjugated *U. europaeus* agglutinin I (UEA-1; red) and fluorescein isothiocyanate-conjugated *G. simplifolia* isolectin B4 (GS-IB4; green). Arrows mark the double staining of UEA-1–stained human and GS-IB4–stained murine blood vessels. (Scale bar: 50 μm.)

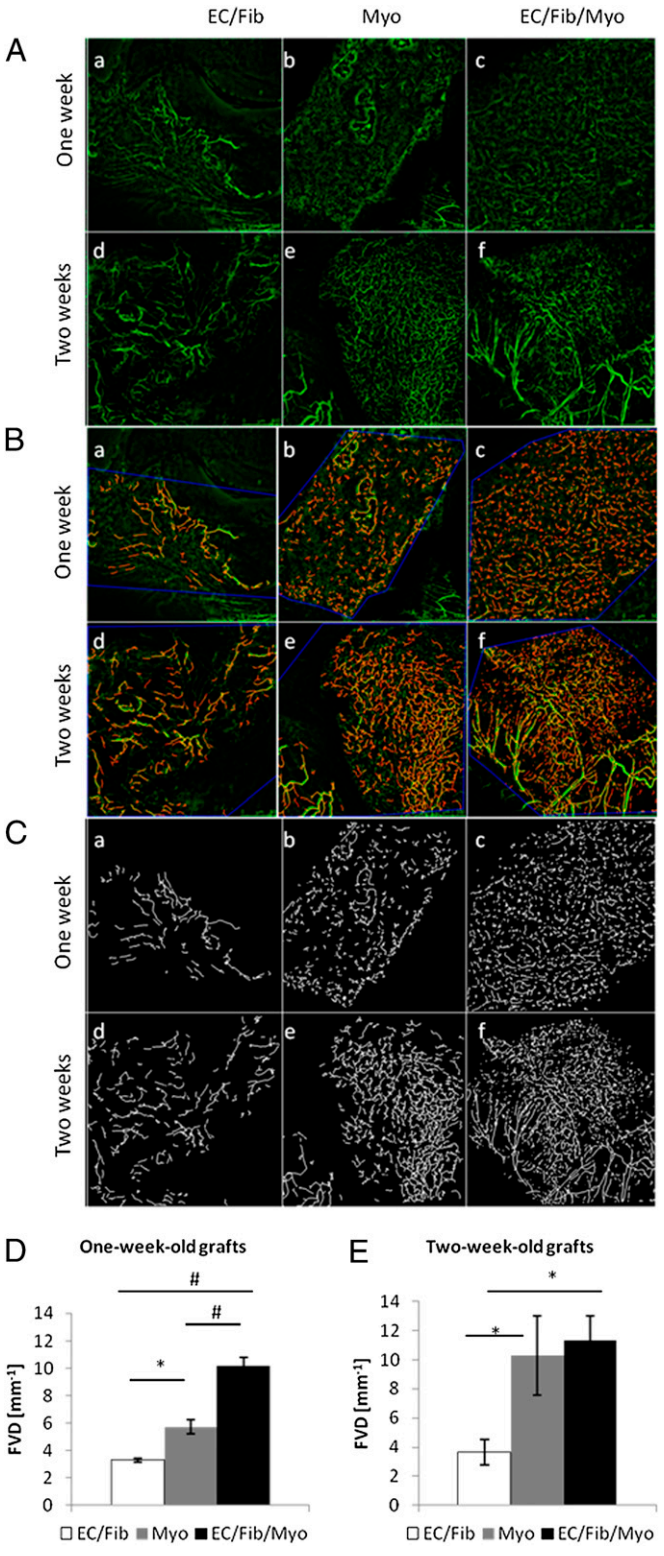

Fig. 3. Representative images of implanted grafts after i.v. injection of FITC-Dextran. (*A*) Confocal images of EC/Fib, Myo, and EC/Fib/Myo grafts taken at varying time points after implantation (a–c, 1 wk; d–f, 2 wk). (*B*) Image processing by MATLAB (a–c, 1 wk; d–f, 2 wk). Blue lines delineate the region of interest in the graft area, red lines delineate the estimated vessel midline, and green is FITC-Dextran. (*C*) Binary image after group size filtering (a–c, 1 wk; d–f, 2 wk). (*D* and *E*) FVD of (*D*) 1- and (*E*) 2-wk-old grafts. $^{*}P < 0.05$; $^{\#}P < 0.01$ according to the results of the posthoc Student Newman–Keuls multiple comparisons test. For all determinations, the sample size was $n \geq 3$, and all values are represented as mean ± SEM.

grafts and Movie S2). At 1 wk postimplantation, both the perfusion rate and the perfused vascular volume within EC/Fib/Myo grafts were higher than those of the Myo and EC/Fib grafts (Fig. 4 *D* and *E*). At 2 wk after implantation, the perfused vascular volume in the EC/Fib/Myo and Myo was higher compared with immediately after the disruption pulse and significantly higher than in EC/Fib grafts, suggesting that the presence of myoblasts promotes graft vasculogenesis. Despite this improved perfused vascular volume, the perfusion rates in the three types of grafts did not significantly differ from one another at this time point (Fig. 4 *F* and *G*).

Flap Transfer and Macroscopic Analysis of the Transferred Flap. We next assessed the viability of the flaps after their transfer to a full-thickness defect in the abdomen (Fig. 1 *J* and *K*). One week after their transfer, flaps derived from cell-populated scaffolds were viable, which was evidenced by their red color (Fig. 1*L*). In contrast, empty scaffolds became necrotic (Fig. 1 *M* and *N*) and in some instances, led to animal death because of herniation of the abdominal organs.

Because most of the functional blood vessels in the transferred flap were of mouse origin, we next determined the extent of flap vascularization by means of murine CD31 staining. Murine CD31- and H&E-stained flap sections revealed the presence of many capillaries within the flaps (Fig. 5 *A–C* and Fig. S3 *A*, *d–f* and *B*, *d–f*). Erythrocytes were seen in the main artery and smaller vessels that supplied the flaps, indicating that the flap vessels remained intact during transfer. When transferred 1 wk after implantation, the extent of vascularization in the EC/Fib/Myo flaps was greater than that of the Myo and EC/Fib flaps (Fig. 5*D*). Moreover, the circumference of vessels in the EC/Fib/Myo flaps was larger than that within EC/Fib flaps (Fig. 5*E*). In contrast, when transferred 2 wk after implantation, the extent of flap vascularization did not significantly differ between the flaps (Fig. 5 *F* and *G*). The extent of vascularization within empty scaffolds was not determined, because they had either necrosed or the mice had died within 2–5 d.

Examination of desmin- and Masson's trichrome (MT) -stained sections revealed that there were 25.2 ± 10.4 and 4.62 ± 3.26 times more desmin-positive staining in the Myo and EC/Fib/Myo flaps than in the EC/Fib flaps 1 and 2 wk postimplantation, respectively (Fig. S3 *A*, *a–c* and *g–i* and *B*, *a–c* and *g–i*). In the EC/Fib flaps, desmin-stained fibroblasts, which had differentiated into smooth muscle cells, were located around CD31-positive vessels (Fig. S3 *A*, *g* and *B*, *g*). MT-stained sections of all flaps transferred 1 wk after graft implantation included myogenic cells at the flap edges proximal to the host tissue (Fig. S3*A*, *a–c*). Examination of the desmin-stained Myo and EC/Fib/Myo flaps transferred at 1 wk postimplantation revealed the presence of myogenic cells also in the center of the flap (next to its vasculature) (Fig. S3*A*, *g–i*). Although most of these myogenic cells were young myoblasts originating from either seeded myoblasts or invading host cells, elongated and aligned myocytes were also observed (Fig. S3 *A*, *h* and *i* and *B*, *h* and *i*). Moreover, most of the myogenic cells in the EC/Fib/Myo flaps were aligned and elongated (Fig. S3*A*, *i*). Examination of the MT- and desmin-stained sections of Myo flaps transferred 2 wk after graft implantation revealed the presence of aligned and elongated myoblasts (Fig. S3*B*, *h*). In the EC/Fib/Myo flaps, mature myocytes, were observed (Fig. S3*B*, *i*), suggesting more efficient integration of EC/Fib/Myo flaps with the host tissue than in other flap types.

Mechanical Flap Properties. During flap extraction attempts 1 wk posttransfer, EC/Fib/Myo flaps showed firm attachment to the surrounding tissue compared with the control groups. In EC/Fib/Myo flap extraction attempts, wound dehiscence did not occur (zero of six), whereas it occurred in 75% of the extraction attempts of the other tested flaps (four of six in Myo flaps and five of six in EC/Fib flaps) and 100% of the attempts made with control grafts

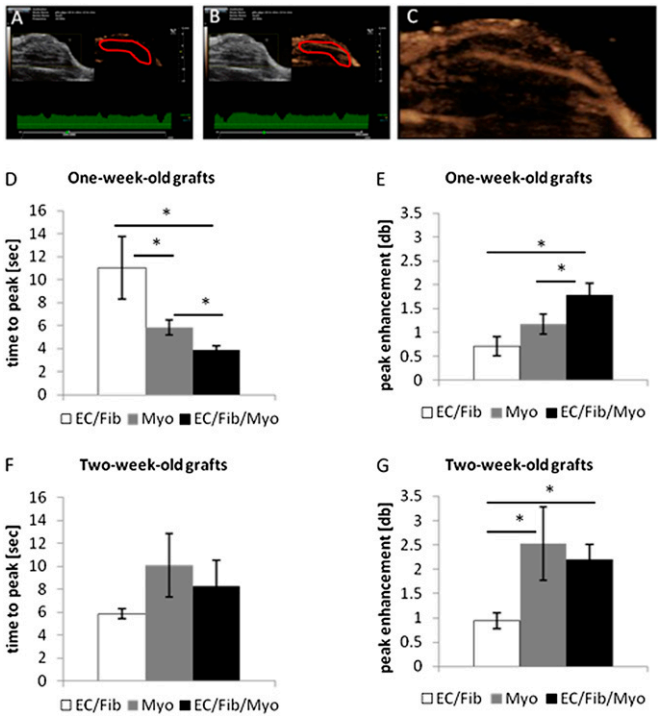

Fig. 4. Ultrasound of EC/Fib, Myo and EC/Fib/Myo grafts after the injection of a contrast agent. (*A–C*) Representative images of the graft after a tail vein injection of microbubble contrast agent. (*A*) Signal immediately after microbubble destruction and (*B* and C) 25 s after the injection the contrast agent. (*A* and *B*) The red outline represents the scaffold area. (*C*) Magnification of *B*. (*D* and *E*) One-week-old grafts. (*F* and *G*) Two-week-old grafts. (*D* and *F*) Blood flow rate in the grafts. (*E* and *G*) Perfusion of the graft. $^{*}P < 0.05$ according to the results of the posthoc Student Newman–Keuls multiple comparisons test. For all determinations, the sample size was $n \geq 3$, and all values are represented as mean ± SEM.

(eight of eight). The engineered flaps were then compared with empty and EC/Fib/Myo control grafts. Hernia was only observed when extracting the empty (three of three) and EC/Fib/Myo grafts (four of five). Evaluation of the tensile strength of the flaps (Fig. 6 *A* and *B*) showed that flaps derived from EC/Fib/Myo scaffolds bore the highest tensile strength (Fig. 6*C*). Myo flap stiffness was greater than that of flaps derived from the empty scaffolds but less than that of EC/Fib flaps (Fig. 6*C*). Similarly, the highest ultimate tensile strength (UTS) was measured for EC/Fib/Myo flaps, whereas flaps derived from empty scaffolds yielded the lowest UTS (Fig. 6*D*). Myo flaps featured a higher UTS than EC/Fib flaps. Overall, these results suggest that the presence of endothelial cells and myoblasts in the flaps is critical for the final strength and stiffness of the fabricated tissue.

Discussion

Reconstruction of complex large soft tissue defects caused by trauma or tumor ablation presents major clinical challenges. Although a wide variety of biological (21–23) and synthetic (1, 24, 25) matrices have been evaluated for their efficacy in tissue repair, their use is limited because of the lack of a blood supply, leading to their necrosis, infection, or possible rejection. In parallel, contemporary surgical techniques exploiting local, regional, or free flaps present disadvantages, such as donor site morbidity, procedure duration, the often scant availability of tissues in the area of the defects, and a requirement for higher surgical skill.

In our previous work (26), we showed that abdominal muscle injuries can be treated using grafts seeded with tricultures of ECs, fibroblasts, and myoblasts. In the present study, we expand the technique to treat large soft tissue defects when skin coverage is inadequate and grafts are ineffective using an engineered tissue with its pedicle. We designed and investigated a novel method for repair of a large soft tissue defect, where an abdominal full-thickness defect was used as a proof of concept using an engineered vascularized flap. The prefabricated graft, implanted around the AV, proved viable, vascularized, and perfused, and it contained blood vessels that anastomosed with host blood vessels. After transfer of the flap to the abdominal wall full-thickness defect, the engineered tissue sample remained viable and vascularized and became well-integrated within the surrounding tissue. EC/Fib/Myo scaffold-derived flaps outperformed all other flap types in their degree of vascularization, perfusion, mechanical properties, and tissue integration within the host. Thus, use of an engineered tissue with a functional blood vessel network can circumvent the need for transfer of massive tissue volumes from another site and avoids postoperative scarification of the donor site.

Proper flap vascularization is essential for its successful integration within the host (24, 25, 27). Various approaches have

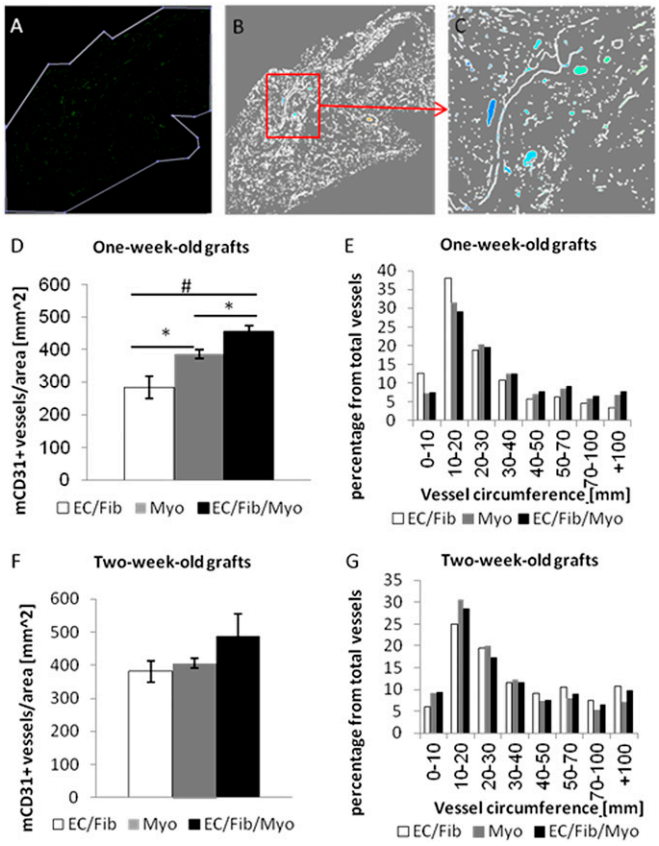

Fig. 5. The extent of vascularization of EC/Fib, Myo, and EC/Fib/Myo flaps as measured by murine CD31 (mCD31) -positive staining. (*A–C*) Image processing of the mCD31-positive vessels by MATLAB. (*A*) White lines delineate the region of interest in the flap. (*B*) Final image after processing. (*C*) Zoomed in view of the selected area in *B*; different colors represent the different circumferences of the blood vessels. (*D* and *E*) Flaps derived from 1-wk-old engineered tissue grafts. (*F* and *G*) Flaps derived from 2-wk-old engineered tissue grafts. (*D* and *F*) mCD31-positive vessels; all values were normalized to the scanned area of the flap in millimeters^2. (*E* and *G*) Histograms of the circumference of the vessels in the flaps (*x* axis) expressed as a percentage of the total number of vessels in the graft (*y* axis). $^{*}P < 0.05$; $^{\#}P < 0.01$ according to the results of the posthoc Student Newman–Keuls multiple comparisons test. For all determinations, the sample size was ≥ 3, and all values are represented as mean ± SEM.

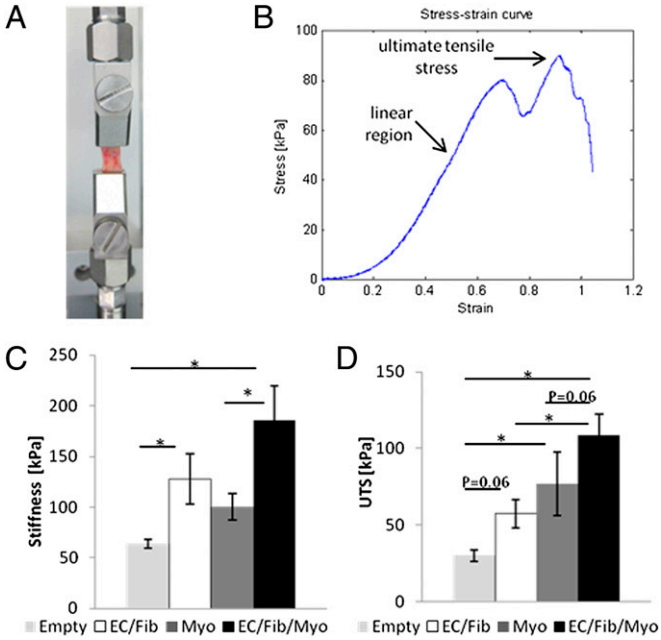

Fig. 6. Mechanical properties of flaps 1 wk after transfer. (*A*) Schematic diagram of a flap being stretched in the Biodynamic test instrument (Bose Corporation). (*B*) A typical stress–strain curve. (*C*) The linear region of the stress–strain curve was used to calculate flap stiffness, and (*D*) the maximum point of the curve was deemed the UTS of the flaps. $*P < 0.05$ according to the results of the one-way ANOVA and the posthoc Student Newman–Keuls multiple comparisons test. For all determinations, the sample size was $n = 3$, and all values are represented as mean ± SEM.

been used to create vascularized engineered tissue to improve oxygen supply and diffusion in thick tissues. Sekine et al. (28) proposed in vitro fabrication of cardiac tissue with perusable blood vessels using a muscle tissue with a connectable artery and vein as a bed perfused in a bioreactor. Dvir et al. (29) constructed a vascularized cardiac patch using both survival and angiogenic factors by first implanting the patch on the omentum. Controlled delivery of proangiogenic factors from growth factor-eluting scaffolds has been shown to induce host vessel ingrowth into the implant (30), whereas EC seeding has been attempted to promote additional vascularization on implantation (31). We have previously shown that the postimplantational vascularization of a scaffold preseeded with ECs and tissue-specific cells was greater than that of EC-free scaffolds and correlated with improved integration within the host tissues (26, 32–35). We have also previously achieved repair of small abdominal defects using an engineered tissue graft derived from a scaffold seeded with HUVECs, fibroblasts, and myocytes (26). However, when fabricated with a viable blood vessel network, larger quantities of tissue and even a whole organ can be implanted and then coupled to the main vessel trunk by attaching the blood vessel network of the engineered tissue to host vessels.

The extensive vascularization and perfusion observed in Myo grafts stands in line with previous reports of secretion of angiogenic factors (including VEGF) by C2C12 cells, which in turn, stimulate vascularization of the surrounding tissue (36, 37). The FVD of Myo grafts, which was higher than that of EC/Fib grafts, was seemingly a result of the large number of small and immature blood vessels, which may have been induced by C2C12-derived angiogenic factors. In parallel, ECs and fibroblasts have also been reported to secrete VEGF (38, 39). In line with these works, the addition of ECs significantly promoted flap vascularization and viability after transfer. We showed that the EC-dependent blood network generated in vitro was functional and integrated with the host vessels on implantation. The EC/Fib/Myo flap underwent the most effective integration and induced the most advanced regeneration of host tissue compared with the other tested flaps. Additional investigation will be necessary to uncover the main role of ECs in viability and integration of engineered tissues (particularly, to determine to what extent the ECs physically participate in blood vessel network formation in vivo and if their impact is primarily through secretion of VEGF and other growth factors after graft transfer) (40).

The presented work shows that the cell types integrated in the engineered flaps dictate their mechanical strength. Specifically, EC/Fib/Myo flaps were stiffer and stronger than EC/Fib, Myo, and empty flaps. We also observed that, during manual flap extraction attempts, wound dehiscence did not occur in mice treated with the EC/Fib/Myo flaps, whereas it often occurred to animals treated with other flaps, which we attribute to the increased mechanical strength of the transplanted tissue (41).

The correlation between secretion of VEGF, a key regulator of myoblast differentiation and function (42, 43), and myoblast maturation has been previously reported (40). When myotubes are formed, the myocytes become vascularized and innervated and finally, mature as myofibers, which are then packed together by connective tissue to provide mechanical strength to the muscle (40, 44–46). Muscle cell alignment and elongation are crucial steps in muscle regeneration, where the final strength of muscle tissue is derived from the parallel organization of the myotubes within the muscle tissue. It has also been shown that vascularization of skeletal muscle is essential for muscle regeneration (47, 48). Indeed, we observed mature and aligned myoblasts in the EC/Fib/Myo flaps, suggesting a mechanism that supports more rapid muscle regeneration.

The results of this study provide experimental evidence for the requirement of tissue-specific cells (i.e., myoblasts) as well as ECs and fibroblasts in successful muscle flap engineering. Furthermore, these results emphasize the need for functional vessels in flaps applied to large soft tissue defects. Specifically, we showed that EC/Fib/Myo flaps became more vascularized by host blood vessels and were more rapidly and more effectively integrated within the host tissue than EC/Fib or Myo flaps. The results of this study are sure to stimulate additional research in a large animal model and clinical studies in humans. In this regard, it is worth mentioning that, in larger animals and humans, other vessels commonly used for reconstruction in the clinic or even engineered large blood vessels can be used for generation of the vascular network of the engineered flap. In addition, the engineered flap can be transferred, as a free flap, to reconstruct defects in other areas of the body.

Materials and Methods

Detailed materials and methods are in *SI Materials and Methods*. Briefly, porous scaffolds were fabricated from 50% PLLA and 50% PLGA as previously described (35). Three types of fabricated grafts were prepared by embedding scaffolds with (*i*) myoblasts (Myo graft), (*ii*) HUVECs and normal human dermal fibroblasts (EC/Fib graft), or (*iii*) HUVECs, normal human dermal fibroblasts, and myoblasts (EC/Fib/Myo graft). Ten days postseeding, mice were anesthetized by an i.p. injection of a ketamine:xylazine (6:1) mixture. The femoral AV bundle was then exposed from the level of the inguinal ligament to the knee area. To preserve the blood flow, the profunda was left untouched. The graft was folded around the exposed femoral AV—below the profunda and above the bifurcation to the tibial and proneal AV—and its ends were joined using 8–0 silk sutures. To ensure implant vascularization by the femoral AV bundle only, a piece of sterilized latex was wrapped around the graft and secured with 8–0 silk sutures. The overlying skin was then closed using 4–0 silk sutures; 1–2 wk after graft implantation, the grafts were either harvested for analysis or transferred as flaps. The tissue flap was then carefully dissected from the surrounding tissues after removal of its latex cover. The distal ends of the femoral AV were ligated with 8–0 silk sutures and then cauterized at the level of the knee (distally to the folded implanted tissue). The femoral AV with the surrounding tissues was then transferred up as a flap to repair a full-thickness defect in the ventral abdominal wall, which was made, during the same procedure, by

removing a 1.0 × 0.8-cm section of the rectus abdominus muscle, with the overlying skin. The flap was sutured to the surrounding muscle tissues using 8–0 silk sutures, and the wound was covered with iodinated gauze and a sterile plaster. The skin of the leg was closed using 4–0 silk sutures. All mice were closely monitored every day for 1 wk, after which time they were euthanized to allow for flap retrieval for tensile strength testing or histological or immunohistological analysis.

ACKNOWLEDGMENTS. The authors thank Dr. Edith Suss-Toby for her assistance with the ultrasound experiments, veterinarians Tali Haas and Michal Schlesinger for their assistance in the animal experiments, and Dr. Arieh Bomzon and Dr. Yehudit Posen for editorial assistance in preparing this manuscript. This research was supported by a Rambam Medical Center Ofakim Grant (to D.E.) and FP7 European Research Council Grant 281501, ENGVASC (to S.L.).

1. Engelsman AF, van der Mei HC, Ploeg RJ, Busscher HJ (2007) The phenomenon of infection with abdominal wall reconstruction. *Biomaterials* 28(14):2314–2327.
2. Vunjak-Novakovic G, et al. (2010) Challenges in cardiac tissue engineering. *Tissue Eng Part B Rev* 16(2):169–187.
3. Laschke MW, et al. (2006) Angiogenesis in tissue engineering: Breathing life into constructed tissue substitutes. *Tissue Eng* 12(8):2093–2104.
4. Polykandriotis E, Arkudas A, Horch RE, Stürzl M, Kneser U (2007) Autonomously vascularized cellular constructs in tissue engineering: Opening a new perspective for biomedical science. *J Cell Mol Med* 11(1):6–20.
5. Guo L, Pribaz JJ (2009) Clinical flap prefabrication. *Plast Reconstr Surg* 124(Suppl 6): e340–e350.
6. Wessells H, McAninch JW (1998) Current controversies in anterior urethral stricture repair: Free-graft versus pedicled skin-flap reconstruction. *World J Urol* 16(3):175–180.
7. Findlay MW, et al. (2011) Tissue-engineered breast reconstruction: Bridging the gap toward large-volume tissue engineering in humans. *Plast Reconstr Surg* 128(6):1206–1215.
8. Pereira LH, Sterodimas A (2008) Free fat transplantation for the aesthetic correction of mild pectus excavatum. *Aesthetic Plast Surg* 32(2):393–396.
9. Haroldo Pereira L, Sterodimas A (2008) Aesthetic restoration of axillary contour deformity after lymph node dissection. *J Plast Reconstr Aesthet Surg* 61(2):231–232.
10. Pereira LH, Sterodimas A (2010) Long-term fate of transplanted autologous fat in the face. *J Plast Reconstr Aesthet Surg* 63(1):e68–e69.
11. Sterodimas A, de Faria J, Nicaretta B, Pitanguy I (2010) Tissue engineering with adipose-derived stem cells (ADSCs): Current and future applications. *J Plast Reconstr Aesthet Surg* 63(11):1886–1892.
12. Mao JJ, et al. (2010) Facial reconstruction by biosurgery: Cell transplantation versus cell homing. *Tissue Eng Part B Rev* 16(2):257–262.
13. Macchiarini P, Walles T, Biancosino C, Mertsching H (2004) First human transplantation of a bioengineered airway tissue. *J Thorac Cardiovasc Surg* 128(4):638–641.
14. Macchiarini P, et al. (2008) Clinical transplantation of a tissue-engineered airway. *Lancet* 372(9655):2023–2030.
15. Atala A, Bauer SB, Soker S, Yoo JJ, Retik AB (2006) Tissue-engineered autologous bladders for patients needing cystoplasty. *Lancet* 367(9518):1241–1246.
16. Nishida K, et al. (2004) Corneal reconstruction with tissue-engineered cell sheets composed of autologous oral mucosal epithelium. *N Engl J Med* 351(12):1187–1196.
17. Petite H, et al. (2000) Tissue-engineered bone regeneration. *Nat Biotechnol* 18(9): 959–963.
18. Banta MN, Kirsner RS (2002) Modulating diseased skin with tissue engineering: Actinic purpura treated with Apligraf. *Dermatol Surg* 28(12):1103–1106.
19. Cheng G, et al. (2011) Engineered blood vessel networks connect to host vasculature via wrapping-and-tapping anastomosis. *Blood* 118(17):4740–4749.
20. Kang KT, Allen P, Bischoff J (2011) Bioengineered human vascular networks transplanted into secondary mice reconnect with the host vasculature and re-establish perfusion. *Blood* 118(25):6718–6721.
21. Patton JH, Jr., Berry S, Kralovich KA (2007) Use of human acellular dermal matrix in complex and contaminated abdominal wall reconstructions. *Am J Surg* 193(3):360–363.
22. Menon NG, et al. (2003) Revascularization of human acellular dermis in full-thickness abdominal wall reconstruction in the rabbit model. *Ann Plast Surg* 50(5):523–527.
23. Buinewicz B, Rosen B (2004) Acellular cadaveric dermis (AlloDerm): A new alternative for abdominal hernia repair. *Ann Plast Surg* 52(2):188–194.
24. Bringman S, et al. (2010) Hernia repair: The search for ideal meshes. *Hernia* 14(1): 81–87.
25. Meintjes J, Yan S, Zhou L, Zheng S, Zheng M (2011) Synthetic, biological and composite scaffolds for abdominal wall reconstruction. *Expert Rev Med Devices* 8(2): 275–288.
26. Koffler J, et al. (2011) Improved vascular organization enhances functional integration of engineered skeletal muscle grafts. *Proc Natl Acad Sci USA* 108(36): 14789–14794.
27. Bellows CF, Alder A, Helton WS (2006) Abdominal wall reconstruction using biological tissue grafts: Present status and future opportunities. *Expert Rev Med Devices* 3(5): 657–675.
28. Sekine H, et al. (2013) In vitro fabrication of functional three-dimensional tissues with perfusable blood vessels. *Nat Commun* 4:1399.
29. Dvir T, et al. (2009) Prevascularization of cardiac patch on the omentum improves its therapeutic outcome. *Proc Natl Acad Sci USA* 106(35):14990–14995.
30. Nillesen STM, et al. (2006) Increased angiogenesis in acellular scaffolds by combined release of FGF2 and VEGF. *J Control Release* 116(2):e88–e90.
31. Chen X, et al. (2009) Prevascularization of a fibrin-based tissue construct accelerates the formation of functional anastomosis with host vasculature. *Tissue Eng Part A* 15(6):1363–1371.
32. Caspi O, et al. (2007) Tissue engineering of vascularized cardiac muscle from human embryonic stem cells. *Circ Res* 100(2):263–272.
33. Lesman A, et al. (2010) Transplantation of a tissue-engineered human vascularized cardiac muscle. *Tissue Eng Part A* 16(1):115–125.
34. Lesman A, et al. (2011) Engineering vessel-like networks within multicellular fibrin-based constructs. *Biomaterials* 32(31):7856–7869.
35. Levenberg S, Golub JS, Amit M, Itskovitz-Eldor J, Langer R (2002) Endothelial cells derived from human embryonic stem cells. *Proc Natl Acad Sci USA* 99(7):4391–4396.
36. Henningsen J, Rigbolt KT, Blagoev B, Pedersen BK, Kratchmarova I (2010) Dynamics of the skeletal muscle secretome during myoblast differentiation. *Mol Cell Proteomics* 9(11):2482–2496.
37. Kanno S, et al. (1999) Establishment of a simple and practical procedure applicable to therapeutic angiogenesis. *Circulation* 99(20):2682–2687.
38. Seghezzi G, et al. (1998) Fibroblast growth factor-2 (FGF-2) induces vascular endothelial growth factor (VEGF) expression in the endothelial cells of forming capillaries: An autocrine mechanism contributing to angiogenesis. *J Cell Biol* 141(7):1659–1673.
39. Ollivier V, Chabbat J, Herbert JM, Hakim J, de Prost D (2000) Vascular endothelial growth factor production by fibroblasts in response to factor VIIa binding to tissue factor involves thrombin and factor Xa. *Arterioscler Thromb Vasc Biol* 20(5):1374–1381.
40. Allbrook D (1981) Skeletal muscle regeneration. *Muscle Nerve* 4(3):234–245.
41. Carlson MA, Chakkalakal D (2011) Tensile properties of the murine ventral vertical midline incision. *PLoS ONE* 6(9):e24212.
42. Claffey KP, Wilkison WO, Spiegelman BM (1992) Vascular endothelial growth factor. Regulation by cell differentiation and activated second messenger pathways. *J Biol Chem* 267(23):16317–16322.
43. Germani A, et al. (2003) Vascular endothelial growth factor modulates skeletal myoblast function. *Am J Pathol* 163(4):1417–1428.
44. Choi JS, Lee SJ, Christ GJ, Atala A, Yoo JJ (2008) The influence of electrospun aligned poly(epsilon-caprolactone)/collagen nanofiber meshes on the formation of self-aligned skeletal muscle myotubes. *Biomaterials* 29(19):2899–2906.
45. Wakelam MJ (1985) The fusion of myoblasts. *Biochem J* 228(1):1–12.
46. Gayraud-Morel B, Chrétien F, Tajbakhsh S (2009) Skeletal muscle as a paradigm for regenerative biology and medicine. *Regen Med* 4(2):293–319.
47. Phillips GD, Schilb LA, Fiegel VD, Knighton DR (1991) An angiogenic extract from skeletal muscle stimulates monocyte and endothelial cell chemotaxis in vitro. *Proc Soc Exp Biol Med* 197(4):458–464.
48. Ota S, et al. (2011) Intramuscular transplantation of muscle-derived stem cells accelerates skeletal muscle healing after contusion injury via enhancement of angiogenesis. *Am J Sports Med* 39(9):1912–1922.

Supporting Information

Shandalov et al. 10.1073/pnas.1402679111

SI Materials and Methods

1. Cell Culture. Myoblasts (C2C12; American Type Culture Collection) were cultured in DMEM (Gibco Life Technologies), which was supplemented with 10% (vol/vol) FBS (HyClone; Thermo Fisher Scientific), 2.5% (vol/vol) Hepes buffer (Biological Industries), 100 U/mL penicillin, and 0.1 mg/mL streptomycin (Pen-Strep Solution; Biological Industries). Human skeletal muscle myoblasts (ScienceCell) were cultured in skeletal muscle cell medium (ScienceCell) supplemented with components of it growth medium. Human umbilical vein endothelial cells (HUVECs; Lonza) and red fluorescent protein-expressing HUVECs (Angio-Proteomie) were cultured in endothelial cell medium and microvascular endothelial cell medium, respectively, supplemented with the components of their respective bullet kits (Lonza). Normal human dermal fibroblasts (NHDFs; Lonza) were cultured in DMEM, which was supplemented with 10% (vol/vol) FBS, 1% nonessential amino acids (Biological Industries), 0.2% β-mercaptoethanol (Biological Industries), and Pen-Strep Solution (Biological Industries). All incubations were performed in a 5% (vol/vol) CO_2 humidified atmosphere at 37 °C.

2. Graft Fabrication. Porous scaffolds were fabricated from 50% poly-L-lactic acid (Polysciences Inc.) and 50% poly(lactic-coglycolic acid) (Boehringer-Ingelheim) in accordance with a previously described protocol (1). Three types of fabricated grafts were prepared by embedding scaffolds [1 cm × 5 mm × 1 mm (length × width × thickness)] with (*i*) myoblasts (Myo graft), (*ii*) HUVECs and NHDFs [endothelial cell (EC)/fibroblast (Fib) graft], or (*iii*) HUVECs, NHDFs, and myoblasts (EC/Fib/Myo graft), which were designed to most closely mimic the composition of muscle tissue. For this purpose, three different cell suspensions were prepared [(*i*) 0.5×10^6 myoblasts in myoblast medium, (*ii*) 0.9×10^6 HUVECs and 0.2×10^6 NHDFs in 1:1 HUVEC:NHDF medium, and (*iii*) 0.5×10^6 myoblasts, 0.9×10^6 HUVECs, and 0.2×10^6 NHDFs in 1:1 HUVEC:myoblasts medium] by growing each cell type separately in its respective medium and preparing each suspension by suspending the cells in a mixture of 4 μL Matrigel and 4 μL culture medium. Each cell suspension was then seeded onto the scaffold and allowed to solidify (30 min, 37 °C, 5% CO_2) in a six-well plate. Cell-free grafts with or without Matrigel were used as controls. After solidification, culture medium (4 mL) was added to each well and replaced every other day for a period of 10 d.

3. Graft Implantation. All animal studies were approved by the Committee on the Ethics of Animal Experiments of the Technion. For all animal-based determinations, athymic nude male mice (7- to 9-wk-old mice; Harlan Laboratories Inc.,) were randomly assigned to three or four groups of three to five mice per group. Before graft (i.e., 10-d-old cell-populated scaffolds) implantation, mice were anesthetized by an i.p. injection (35 μL/20 g) of a ketamine:xylazine (6:1) mixture. The femoral artery and vein (AV) bundle was then exposed from the level of the inguinal ligament to the knee area. To preserve the blood flow, the profunda was left untouched. The graft was folded around the exposed femoral AV (below the profunda and above the bifurcation to the tibial and proneal AV), and its ends were joined using 8–0 silk sutures. To ensure implant vascularization by the femoral AV bundle only, a piece of sterilized latex was wrapped around the graft and secured with 8–0 silk sutures. The overlying skin was then closed using 4–0 silk sutures. All mice were monitored closely until they recovered from the anesthesia and every day thereafter until the grafts were harvested for analysis or transferred as flaps.

4. Flap Transfer. Mice were anesthetized with the ketamine:xylazine mixture 1–2 wk after graft implantation. The tissue flap was then carefully dissected from the surrounding tissues after removal of its latex cover. The distal ends of the femoral AV were ligated with 8–0 silk sutures and then cauterized at the level of the knee distally to the folded implanted tissue. The femoral AV with the surrounding tissues was then transferred up as a flap to repair a full-thickness defect in the ventral abdominal wall, which was made during the same procedure by removing a 1.0 × 0.8-cm section of the rectus abdominus muscle with the overlying skin. The flap was sutured to the surrounding muscle tissues using 8–0 silk sutures, and the wound was covered with iodinated gauze and a sterile plaster. The skin of the leg was closed using 4–0 silk sutures. Cell-free and EC/Fib/Myo grafts were used as control groups. EC/Fib/Myo grafts were incubated for the whole period in vitro (24 d). In the control groups, the grafts were sutured to repair a full-thickness defect in the abdominal wall (as explained above) without transferring the femoral AV. All mice were closely monitored every day for 1 wk, after which time they were euthanized to allow for flap retrieval for tensile strength testing (see below) or histological or immunohistological analysis.

5. Determination of the Extent of Functional Graft Vascularization. The extent of tissue graft vascularization was determined 1 and 2 wk after implantation. After anesthetization with ketamine and xylazine, 10 mg/mL FITC-Dextran (Sigma-Aldrich) was i.v.-injected into the tail vein. On completion of the injection, the mice were euthanized, and the graft was imaged using confocal microscopy. The grafts were then excised and transferred to 10% buffered formalin (Sigma-Aldrich) for histological or immunohistological analysis.

Vascularization was quantified using MATLAB (Mathworks). First, the green channel (excitation = 488 nm) of the confocal microscopic images was isolated. The resulting images were then passed through a high-pass filter to accentuate the high-contrast structures. Second, a despeckling filter was used to remove noise that might have been amplified by the high-pass filter. The resulting image was then thresholded using a predefined value; the threshold value was adjusted so that the features and structures in the original image were visible in the binary image. A size threshold was then applied so that only groups of connected pixels larger than the size threshold remained in the binary image. Finally, the skeleton of the vessels in the graft was outlined using Zhang–Suen's algorithm to determine the functional vessel density (FVD) in each graft. The FVD was calculated by summing the lengths of the midline of each vessel and dividing the result by the area of the region of interest (ROI).

6. Ultrasound Determination of Vascular Perfusion of the Graft. Before transfer, vascular perfusion of the graft was measured 1 and 2 wk after implantation by ultrasonography. For this purpose, mice were anesthetized using 2% isoflurane; animal body temperature was maintained using a movable heated stage (VisualSonics) with temperature that was set at 38 °C. Patency of the femoral vessels was examined, and the grafts were first located using B-mode and color Doppler ultrasonography (Movie S1), with an MS250 nonlinear transducer (VisualSonics). Then, the Vevo Micromarker nontargeted contrast agent (microbubbles; VisualSonics) was injected into the tail vein. Images were captured

in the nonlinear contrast mode of the Vevo 2100 high-resolution ultrasound system and analyzed using the Vevo 2100 software as described previously (2). Briefly, an ROI was drawn on the graft's image that was obtained from B- and contrast-mode images that were captured immediately after a disruption pulse, which destroys all of the injected microbubbles. After the disruption pulse, the microbubbles refill the vessels at a rate that only depends on the flow rate of the microbubbles in the capillaries and is independent of the injection rate of the microbubbles. The peak enhancement is the ratio of the mean intensity of the nonlinear signal after the injection of the microbubbles vs. after the disruption pulse, and it is a measure of the perfusion volume. The flow rate can be determined from the time that elapses until the peak signal. Patency of the femoral vessels posttransfer was ensured using the Doppler mode.

7. Immunohistological and Histological Staining of the Grafts and Flaps. Grafts were fixed in 10% neutral buffered formalin (Sigma-Aldrich) and embedded in paraffin using standard fixation and embedding procedures. The paraffin-embedded sections were then deparaffinized by immersion in 100% xylene and rehydrated by serial immersions in decreasing concentrations of ethanol. Standard protocols were used for H&E and Masson's trichrome staining of the paraffin-embedded sections. For immunohistological staining, the epitopes were recovered by heating the specimens in Vector antigen unmasking solution (Vector Laboratories). The activity of endogenous peroxidase was quenched by incubating the slides in 3.3% (vol/vol) H_2O_2 solution in methanol for 10 min, rinsing in PBS, and then incubating in a 2% (vol/vol) goat serum blocking solution for 30 min at room temperature (RT). The slides were then incubated overnight at 4 °C in an anti-CD31 antibody solution (1:50; Abcam), rinsed with PBS, incubated with a biotinylated secondary antibody (1:400; Vector Laboratories) for 30 min at RT, rinsed with PBS, and incubated with streptavidin-peroxidase (1:400; Vector Laboratories) for another 30 min at RT. The nuclei were stained in blue by immersing the sections in hematoxylin for 2 min. After gentle rinsing in water, the sections were covered with Vectamount mounting medium (Vector Laboratories). CD31 staining was visualized as a brown stain using the aminoethylcarbazole substrate kit (Invitrogen). CD31-positive staining was determined and quantified in a double blind analysis of five randomly selected areas within the graft observed at 40× magnification.

The tissues were harvested and fixed in 4% paraformaldehyde (Electron Microscopy Sciences) for 1–2 h, incubated overnight in a 30% (wt/vol) sucrose solution, embedded in optimal cutting temperature compound (Tissue-Tec), and frozen for subsequent cryosectioning (5–7 μm). The sections were incubated in a 0.5% Tween solution for 20 min, rinsed with PBS, and then blocked with a 5% (wt/vol) BSA (Sigma-Aldrich) blocking solution for 30 min. The sections were then simultaneously incubated in an anti-CD31 antibody solution (1:200; BD Biosciences) and an anti-desmin antibody solution (1:50; Santa Cruz Biotechnology, Inc.) for 30 min at RT before being thoroughly washed in PBS. The sections were then labeled with Alexa 488 and Alexa 532 dye conjugates of IgG (1:200; Jackson Immunoresearch Laboratories, Inc.). The slides were mounted in Vectashield that contained DAPI (Vector Laboratories) before being examined under a fluorescence microscope (Axiovert 200M; Zeiss) and a Leica TCS-LSI confocal microscope.

8. Determination of the Extent of Flap Vascularization and Vessel Circumference. The extent of flap vascularization and vessel circumferences were determined by quantifying CD31 staining. For this purpose, flap cryosections were first immunostained for murine CD31, which was quantified using the tile function of the Leica TCS-LSI confocal microscope and a MATLAB code. The code first filtered the green (excitation = 488 nm) channel from the image to isolate the murine CD31 staining. An automatic image analysis process was then used to segment the blood capillaries in a given ROI and calculate the area and circumference of the segmented vessels. The image segmentation was performed as follows. Single images taken from the TIF stack sequence input, which was created by the confocal microscope's software, were first summed. Median image filtration was then applied to reduce noise before manual masking of the ROI. The resultant image was converted into a binary image, and Sobel edge filtering was applied to detect the edges of the capillaries. This image of the edges was segmented using morphological operators, which enhanced and connected the edges of the vessels. Dilation was used to intensify and connect the vessels, and a dilation operator was used to reduce noise and delete small pixel elements. The image, now showing only the intensified edges of the vessels, was analyzed using an eight-neighbor boundary detection algorithm that generated a single vector graphics representation for each closed vessel. The area and circumference of each vessel were calculated and written into a CSV text file, which was used for the final analysis. In this analysis, vessels with small lumens (circumference < 8 pixels) were categorized as noise and disregarded in the final analysis.

9. Determination of the Extent of Vascular Anastomosis. To distinguish between host vessels and the implanted HUVECs and determine whether the vessels had anastomosed, a mixture of rhodamine-labeled *Ulex europaeus* agglutinin I (Vector Laboratories) human-specific lectin and FITC-conjugated *Griffonia simplifolia* isolectin B4 (Vector Laboratories) murine-specific lectin were injected into the tail vein 1 wk after graft implantation using a previously described protocol (2). Mice were euthanized 20 min after the injection, and the grafts were harvested, fixed in 10% buffered formalin for 2–4 h, incubated overnight in 30% (wt/vol) sucrose, embedded in optimal cutting temperature compound, frozen, and cryosectioned into 60-μm sections for confocal imaging.

10. Tensile Testing of the Flaps. A stress–strain curve was generated using the Biodynamic test instrument (Bose Corporation) under a strain rate of 0.01 mm/s until failure. Stress was calculated as the measured force divided by the cross-sectional area of the flap, and strain was calculated as elongation divided by the flap's initial length. The flap's stiffness was calculated as the slope of the linear region of the stress–strain curve, and the maximum point of the curve was deemed to be the ultimate tensile strength (3). For these determinations, the flaps were retrieved 7 d after transfer, and their dimensions were obtained while they were maintained in PBS and immediately after mounting them onto the system's grips.

11. Statistical Analysis. All data were statistically analyzed by a one-way ANOVA followed by a posthoc Student Newman–Keuls multiple comparisons test using a computerized statistical program (InStat; GraphPad Software, Inc.). Statistical significance was set at 5%, and all results are presented as mean ± SEM.

1. Levenberg S, Golub JS, Amit M, Itskovitz-Eldor J, Langer R (2002) Endothelial cells derived from human embryonic stem cells. *Proc Natl Acad Sci USA* 99:4391–4396.
2. Meintjes J, Yan S, Zhou L, Zheng S, Zheng M (2011) Synthetic, biological and composite scaffolds for abdominal wall reconstruction. *Expert Rev Med Devices* 8(2):275–288.
3. Claffey KP, Wilkison WO, Spiegelman BM (1992) Vascular endothelial growth factor. Regulation by cell differentiation and activated second messenger pathways. *J Biol Chem* 267(23):16317–16322.

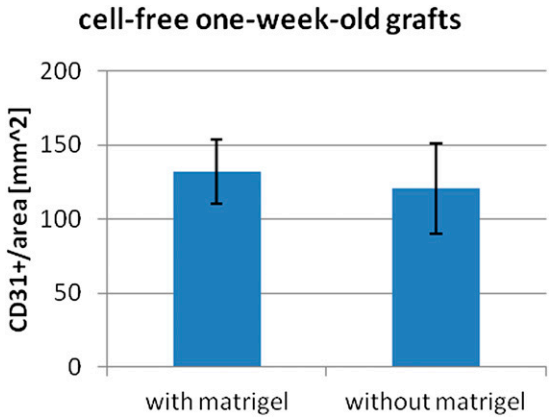

Fig. S1. Comparison between cell-free grafts in the presence or absence of Matrigel. CD31-positive staining of cell-free 1-wk-old grafts in the presence or absence of Matrigel ($n = 3$; no significant difference).

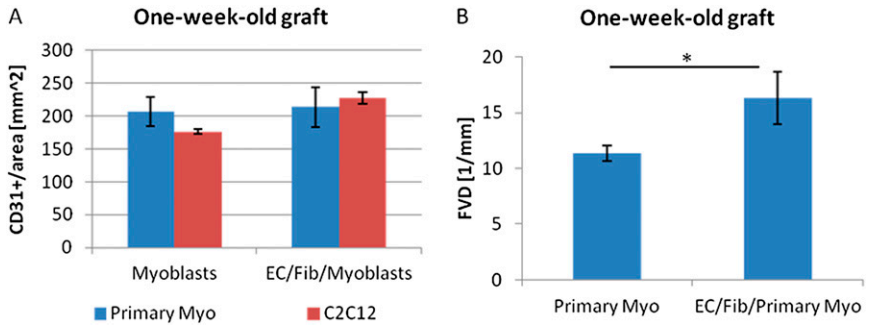

Fig. S2. Comparison between primary myoblasts and C2C12 myoblasts. (*A*) CD31-positive staining of EC/Fib/Myo grafts embedded with C2C12 (red) vs. primary myoblasts (blue). (*B*) FVD of primary myoblasts and EC/Fib/Primary Myo of 1-wk-old grafts. *$P < 0.05$ ($n = 3$ for all groups).

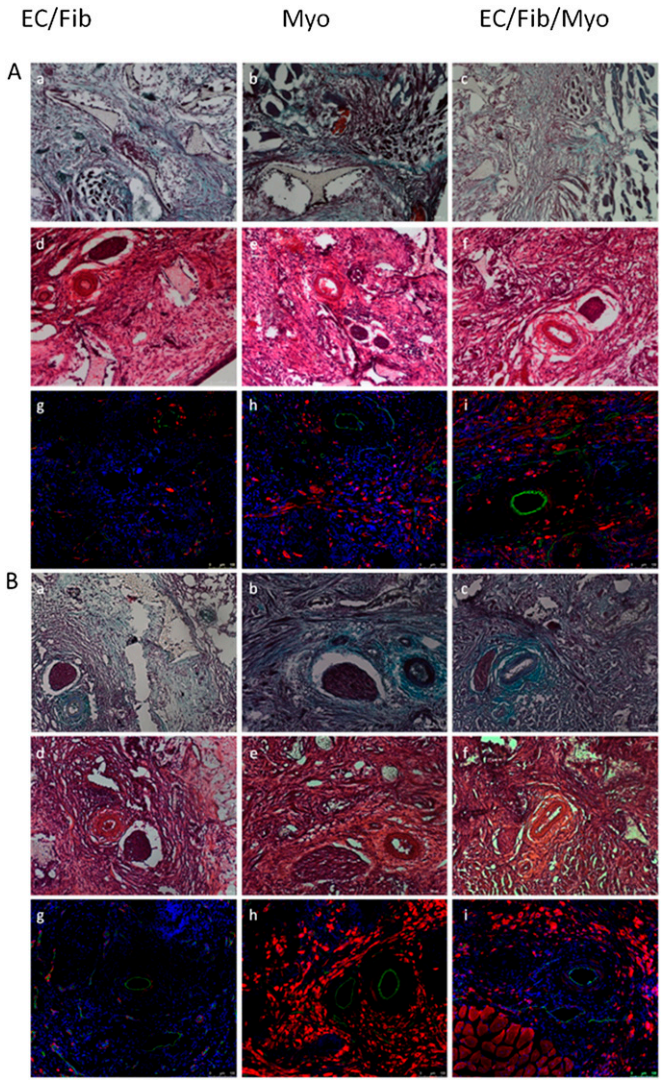

Fig. S3. Representative images of histological staining of transferred flaps. Flaps transferred (*A*) 1 or (*B*) 2 wk postimplantation. (*a–c*) Masson's trichrome staining (×10). (Scale bar: 100 μm.) (*d–f*) H&E staining (×10). (Scale bar: 100 μm.) (*g–i*) Immunofluorescent staining: murine CD31-positive staining (green) and desmin-positive staining (red). The nuclei are stained blue. (Scale bar: 100 μm.)

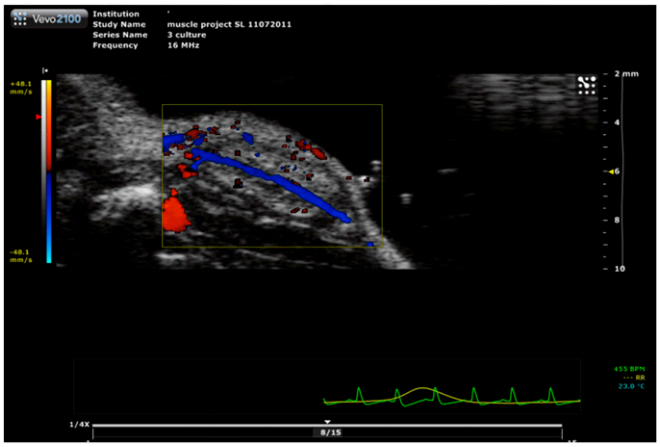

Movie S1. Doppler movie of 2-wk-old EC/Fib/Myo graft. Blue and red staining indicates blood flow. Two weeks postimplantation, the AV is potent, which is indicated by the blood flow in the AV located in the center of the graft.

Movie S1

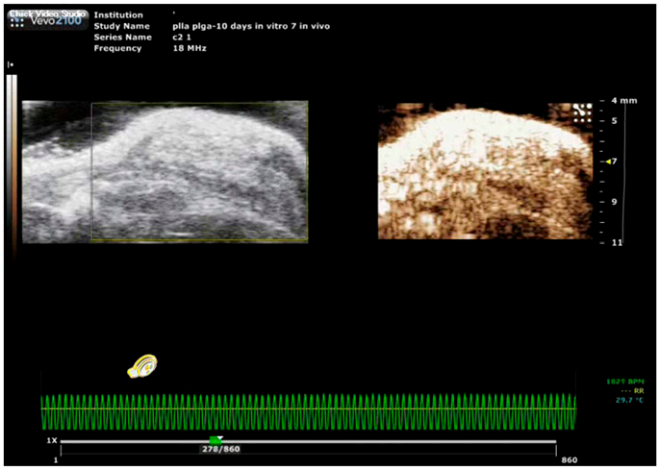

Movie S2. Ultrasound movie of contrast agent injection into a 1-wk-old Myo graft. The contrast agent can be evaluated by the expression of the low number of orange pixels within the graft immediately after the disruption pulse of the microbubbles and signal increase with time. The graft is filled from the AV (located in the center of the graft). (*Left*) B-mode movie of the graft. (*Right*) Contrast movie of the graft.

Movie S2